Giant configurational softening controls atomic-level process of shear banding in metallic glasses

Zeng-Yu Yang [1,2] and Lan-Hong Dai [1,2,3,*]

[1] *State Key Laboratory of Nonlinear Mechanics, Institute of Mechanics, Chinese Academy of Sciences, Beijing 100190, China*
[2] *School of Engineering Science, University of Chinese Academy of Sciences, Beijing 100049, China*
[3] *School of Future Technology, University of Chinese Academy of Sciences, Beijing 100049, China*

(Received 23 August 2021; accepted 19 November 2021; published 6 December 2021)

While the shear banding is a ubiquitous feature for metallic glasses and other disordered solids, the underlying material softening mechanism is still an open question requiring physical interpretation at atomic level. Here, through a set of atomistic simulations, we clarify the origin of flow localization, i.e., the birth of a shear band. The local thermal temperature induced by atomic vibration and configurational temperature attributed to structural disordering are proposed to quantify critical degree of thermal and configurational softening, respectively. The comparison between configurational softening and thermal softening being two potential causes for shear banding emergence is then examined at atomic scale. Numerical evidence from atomistic simulations indicates that configurational-softening-induced strain burst is the dominant instability mode as evidenced through a very large value of configurational temperature rise that commensurate with glass transition temperature. It is also found that configurational softening takes precedence over thermally activated ones. Configurational softening is thus conceivably acting as the root cause for the onset of strain localization and shear banding, while the subsequent thermal softening is its consequence. These results provide important insights into the puzzle about the material weakening mechanism underlying shear banding.

DOI: 10.1103/PhysRevMaterials.5.123602

I. INTRODUCTION

For a variety of amorphous solids, especially metallic glasses (MGs), shear banding with severe localized deformation burst in exact thin regions is a prevalent and fundamental phenomenon [1,2]. The shear band phenomenon usually causes catastrophic failure that is harmful to the engineering utilities of structural materials, which require robustness to different kinds of mechanical loadings. The origin of shear banding or strain localization, usually in the form of aggregation of shear transformation zones [3,4], is a self-feedback state [5,6] in which the onset of local plastic flow is triggered by a softening mechanism acting to preferentially accommodate further strain in the exact local region. A thorough understanding of the softening mechanism is thus of the primary scientific interest for plastic deformation in MGs.

In crystalline alloys, shear banding is widely accepted as the consequence of thermal-plastic instability [7]. For metallic glasses, however, there are two views taking the shear bands as either thermal induced [8] or by virtue of configurational softening [9], leading to a continuing controversy [2]. To solve this puzzle, extensive research efforts have been made to know the temperature rise in shear bands. In terms of theoretical analysis, Langer and coworkers [10–14] established a constitutive model describing the deformation process via two different temperatures: thermal temperature and effective disorder temperature. On the basis of such concept, our following theoretical works found that temperature rise lags behind the local free volume creation as well as the increment of effective temperature [15–17]. This point is verified by experimental observations under various loading conditions [18–20], which induce the propensity to demonstrate that configurational softening is the dominant contributor, whereas the thermal softening plays insignificant role in shear banding of metallic glasses. In addition, the answer to the question "Must shear bands be hot?" [21] has been further given by the very recent simulation work [22]. In Ref. [22], athermal quasistatic shear loading is used to rules out the effect of local heating. The observation of strain localization as well as shear banding in such athermal conditions is thus the direct evidence that the phenomenon of strain-softening, leading to shear bands can take place without temperature.

Despite these excellent theoretical, experimental and simulated works, the microscopic mechanism underlying softening history during deformation process is still an open question since the existing concepts of effective or fictive temperature are usually used as global properties [23,24]. However, due to the intrinsic localized nature of shear banding, there is also a pressing need of microscopic mechanism tracing back to the possible atomic scales. To address this issue, the atomic thermal temperature and in parallel, configurational temperature are proposed in the present work to measure the critical level of thermal-induced softening and configurational-induced softening under external loading. These definitions permit to quantitatively capture the spatial and temporal evolution of local configurational softening and thermal softening, respectively. On the basis of these definitions, an in-depth understanding of softening mechanism with unprecedented spatial and temporal resolution is given, which reinforces the dominant role played by local configurational softening.

*lhdai@lnm.imech.ac.cn

II. SIMULATION DETAILS

Due to the extremely short timescales of shear localization, we utilize the powerful molecular dynamics (MD) simulations, where we can attain the state at the onset of shear band for analysis. All of the MD simulations are conducted using the open source LAMMPS code [25]. We consider a prototypical binary system $Cu_{50}Zr_{50}$ with a size of 35 nm × 35 nm × 7 nm, containing ∼500 000 atoms. Here atoms interact with each other through the embedded-atom method potential [26]. For the process of glass preparation, a small sample containing 19 652 atoms is first melted from its crystalline phase from 50 K to 2050 K and then equilibrated for 500 ps at 2050 K. Such fully equilibrated melting liquid is then quenched to a glassy state with a slowest possible cooling rate of 10^9 K/s. The larger model system to be deformed is then produced by the replication of the initial glass configuration. The large system is further relaxed for 500 ps at 800 K to reduce the artificial boundary effect of multiplication. Isothermal-isobaric ensemble (N atom number, P pressure, and T temperature) using Nose-Hoover thermostat [27] is employed to control the pressure and temperature during glass preparation process. At deformation state, however, the thermostat is turned off so that it would not artificially affect the increase of local temperature [28]. Simple shear loading, with prescribed constant strain rate 10^8 s^{-1} is used to capture the inhomogeneous deformation. Periodic boundary conditions are applied for all the simulations. The MD time step is 0.002 ps to numerically integrate Newton's equation of motion.

III. RESULTS AND DISCUSSIONS

A. Results of molecular dynamics simulations

We now present the result of atomistically deforming simulations. The overall shear banding evolution of $Cu_{50}Zr_{50}$ MG under external loading is illustrated by the shear stress-strain curve as shown in Fig. 1. The sample stress shows elastic behavior up to the onset of yielding at strain of 0.1. As deformation goes on, the stress exhibits a drastic decrease, i.e., stress overshoot in shear, which points out the appearance of strain localization [29–31]. Here the formation of shear band falls behind at a later strain of 0.12, after which the model glass develops into plastic flow stage with the formation of mature shear band. The heterogeneous manner of deformation is revealed via spatial distribution of plastic events quantified by nonaffine displacement $D^2_{\min}$ [4], as seen in the insets of Fig. 1. Regions with relatively large value of $D^2_{\min}$ make up the well-defined shear transformation zones (STZ) [32,33]. At initial deformation, STZs pop up in various locations that are soft enough and free of shear resistance [34,35]. As deformation evolves further, neighboring shear transformations accompanied by local density changes [36], can be aggregated in an autocatalytic manner, thus percolating into the ultimate shear band [6].

B. Definition of atomic thermal temperature

Next, we demonstrate the softening history that induces a shear band. To address this issue, two coefficients that quantify critical degree of thermal- and configurational-induced

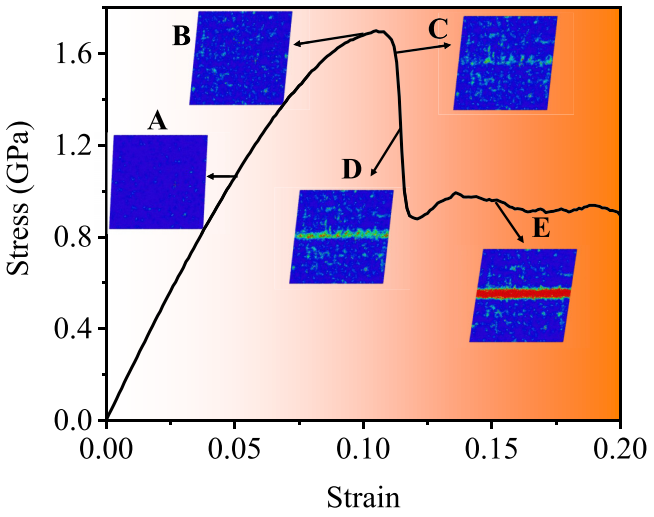

FIG. 1. The stress-strain curve of $Cu_{50}Zr_{50}$ metallic glass under strain rate of 10^8 s^{-1}. The insets A–E are deformation patterns at strain of 0.05 (initial deformation), 0.10 (elastic limit), 0.112 (shear localization), 0.114 (shear banding formation), and 0.15 (plastic flow), respectively. Here atoms are colored according to the magnitude of $D^2_{\min}$ with color scale ranging from 0 Å^2 (blue) to 5 Å^2 (red).

softening burst are defined onto each atom. First, the atomic thermal temperature is defined according to the kinetic energy per atom, normalized to give a temperature in Kelvin:

$$T_t^i = \tfrac{2}{3}E_{ke}^i/k_B, \tag{1}$$

where T_t^i and E_{ke}^i denote thermal temperature and kinetic energy for ith atom, respectively, and k_B is Boltzman constant. In order to give a meaningful temperature with sufficient self-averaging [28], we consider nonlocal manners that has been proved as the nature of many glassy properties [37,38]. The collective local softening and plastic events containing atoms spanning from dozens to hundreds are not exactly controlled by the first-shell local structure, but rather their structural fingerprint is embedded in several shells of the radial distribution function (RDF) via spatial correlations. Here spatial coarse graining is used and we define the average local thermal-temperature with motivation from Ref. [39]. The formalism is as follows:

$$\bar{T}_t^i = \frac{\sum_j T_t^j f(r_{ij}) + T_t^i}{\sum_j f(r_{ij}) + 1}, \tag{2}$$

where j is the atomic id for neighbors around atom i and $f(r_{ij})$ is a switching function:

$$f(r_{ij}) = \frac{1-(r_{ij}/r_c)^N}{1-(r_{ij}/r_c)^M}. \tag{3}$$

Here r_{ij} is the distance between central atom i and its neighboring particle j. We set $N = 6$ and $M = 12$ as it is done in Ref. [39]. Thus the switching function is a form of smooth decay function, with $f(r_{ij}) \approx 1$ for $r_{ij} \ll r_c$ and $f(r_{ij}) \approx 0$ when $r_{ij} \gg r_c$. Since it considers the attenuation of spatial correlation when distance between central atom and neighboring ones is increasing, such a form is more efficient when

compared with purely spatial average and has been proven useful in crystalline and disordered materials [39]. The cut-off distance r_c is chosen to be 6 Å which corresponds to the location of second valley in the RDF. Here the RDF of configurations at different macroscopic strains are plotted in Appendix A. It is therefore the atomic thermal temperature is coarse grained and contains short-range and medium-range interactions.

C. Definition of atomic configurational temperature

In parallel, the configurational temperature is defined as the derivative of the configurational potential energy with respect to the configurational entropy. In order to use this parameter as a local indicator, we have to project it onto each atom. Of course configurational potential energy $E_{\rm pe}$, is easy to estimate by using the empirical potential function and atomistic simulations. As there is no exact expression for configurational entropy, it is an extreme challenge to evaluate. However, in terms of liquid state theory, an expanding expression with an infinite series of terms concerning multibody correlation functions is derived [40]. The first term of this expression, S_2, including pair correlations has the form of

$$S_2^i = -2\pi\rho \int_0^\infty [g^i(r)\ln g^i(r) - g^i(r) + 1]r^2 dr. \quad (4)$$

Here S_2^i is the configurational entropy for ith atom. ρ is the number density of the system. $g^i(r)$ [39] is the atomic RDF centered at atom i. Equation (4) gives an approximate evaluation and is adequate to account for about 90% of the configurational entropy in simple liquids and amorphous solids [41]. Such local structural entropy S_2^i positively correlates with plastic flow [42] and is extensively used as structural fingerprint for crystalline materials [39] as well as disordered solids such as metallic glasses [43] and colloidal glasses [33]. Thus, this term is sufficient for the purpose of probing the configurational softening process under external mechanical stimuli. Then we can write the atomic configurational temperature as $k_{\rm B}T_{\rm c}^i = \partial E_{\rm pe}^i/\partial S_2^i$. It can be approximated by the numerical differentiation method:

$$T_{\rm c}^i = \frac{1}{k_{\rm B}}\frac{\Delta E_{\rm pe}^i}{\Delta S_2^i} \simeq \frac{1}{k_{\rm B}}\frac{\left|E_{\rm pe}^i(t+\Delta t) - E_{\rm pe}^i(t)\right|}{\left|S_2^i(t+\Delta t) - S_2^i(t)\right| + \delta}, \quad (5)$$

in cases that the time interval Δt is small enough. Here Δt is set as 10 ps, such a short timescale means 0.001 increment in sample strain for our loading simulation with strain rate of 10^8 s^{-1}. The positive δ is a correction factor used to prevent divergence of results for minority of atoms that retain the exact same S_2^i at time t and $t + \Delta t$. We set $\delta = 0.1$ which is some two order of magnitude less than the absolute value of S_2^i, thus making sure the validity of our results below. Like the definition of $\bar{T}_{\rm t}^i$, we also use the coarse graining procedure in Eq. (2), and define the local configurational temperature $\bar{T}_c^i$. It should be noted that similar definitions, namely effective temperature [44] or fictive temperature [45], have been introduced as global properties in previous theoretical models [10–12] as well as simulated and experimental results [23,24,46] concerning thermodynamics in disordered materials. While these concepts have achieved great success in demonstrating nonequilibrium dynamics of glasses, they still have limitations in getting insight into atomic-level events. In this connection, the configurational temperature proposed in the present work is a substantial extension of these existing protocols to atomic scale. As a further step beyond the effective temperature or fictive temperature, atomic configurational temperature can be used to explore, with unprecedented precision and spatial resolution down to atomic scale, the softening process induced by local structural changes and disordering procedures.

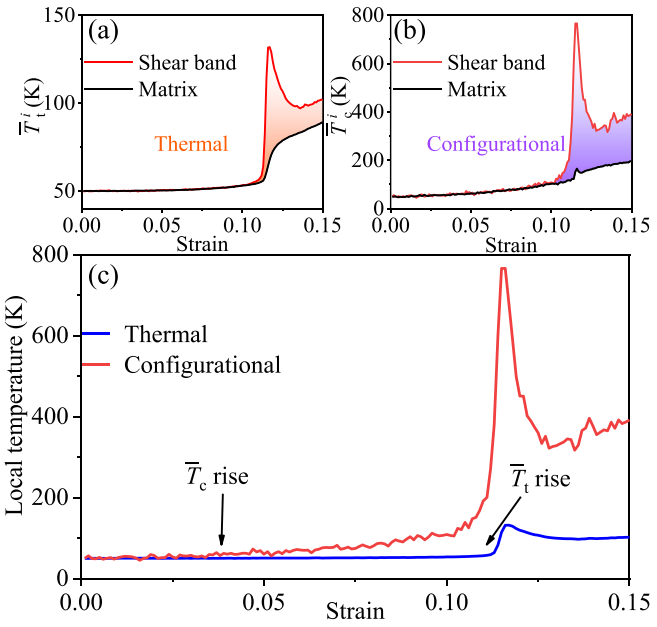

FIG. 2. Softening localization during shear banding process. Evolution of local thermal temperature $\bar{T}_{\rm t}^i$ (a) as well as configurational temperature $\bar{T}_{\rm c}^i$ (b) in shear band and the surrounding matrix. (c) Direct comparison of evolution of thermal softening and configurational softening in the shear band.

D. Comparison between thermal softening and configurational softening

Having identified the basic softening mode as thermal- and configurational-induced, it is now possible to discuss the softening history before the onset of shear banding in detail. We address this issue by tracking the evolution of atomic thermal and configurational temperature. It should be noted that the calculated configurational temperatures have been normalized to 50 K at the initial state to make it convenient to compare with thermal temperature. Here the statistic $\bar{T}_{\rm t}^i$ and $\bar{T}_{\rm c}^i$ as a function of macroscopic strain is given in Figs. 2(a) and 2(b). The results are calculated for atoms in and outside the shear band (see Appendix B for the details of identification of shear band region). Intuitively, the mismatch between shear band and surrounding matrix is obvious for both of $\bar{T}_{\rm t}^i$ and $\bar{T}_{\rm c}^i$. However, the $\bar{T}_{\rm t}^i$ rise, at the stage of localization, is less than 100 K (initial temperature is 50 K) which is much smaller than the temperature needed to cause thermal-induced glass transition at the timescale considered in this study. Thus the band remains cold in this regard. For comparison, the observed rise of configurational temperature inside shear band is

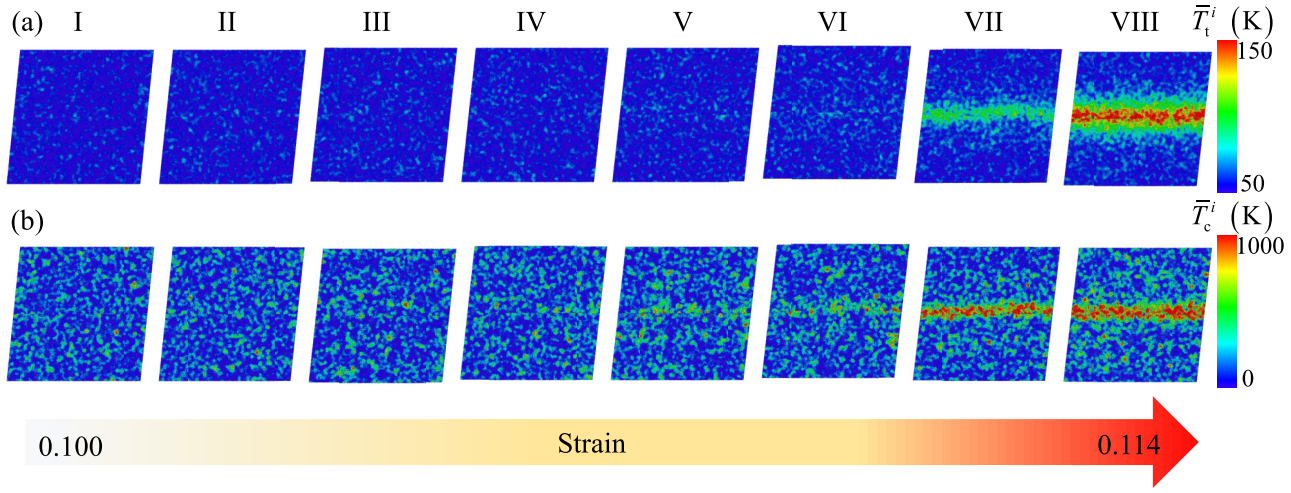

FIG. 3. Projected views of the atomic configurations during deformation. I–VIII display the spatial distributions of atomic thermal temperature (a) and configurational temperature (b) at various shear strains just before the formation of mature shear band. The strain ranges from I to VIII is from macroscopic strain of 0.1 to 0.114, with strain interval between the successive frames is 0.002.

much higher than that of thermal temperature. This indicates that configurational softening is expected to be the dominant processes for shear banding. This result is also consistent with recent long timescale simulations which indicate that homogeneous plastic flow is usually dominated by thermally activated diffusion, whereas local structural instability in the form of shear banding retains an athermal nature [47,48]. Moreover, it is of note that the maximum value of $\bar{T}_c^i$ in the shear band reaches nearly 800 K. Since the configurational temperature at initial state is reduced to 50 K, the maximum rise of $\bar{T}_c^i$ inside the shear band is thus ∼750 K, which is slightly above the glass transition temperature (for this system, the glass transition temperature is nearly 650 K). On the basis of this result, it is reasonable to speculate that the shear banding behavior of metallic glasses is indeed the glass-liquid transition induced by configurational softening. This point is in striking agreement with Ref. [22], which shows that the glass state inside the shear band, as measured by the distribution of local yield stress [49–51], is comparable with that of inherent structures obtained by instantaneously quenching liquids from a temperature slightly higher than the glass transition temperature.

To further compare explicitly the susceptibility of thermal temperature and configurational temperature under deformation, we plot the evolution of $\bar{T}_t^i$ and $\bar{T}_c^i$ together as shown in Fig. 2(c). During shear localization process, the rise of configurational temperature occurs indeed prior to the increase in local thermal temperature. It shows that configurational softening displays a growth trend upturn at strain of 0.04 much earlier than strain localization, while the thermal activation occurs after the onset of yielding. It is the direct evidence that the former is the origin of shear banding, whereas the latter is its consequence. This result is in line with recent excellent experimental works [52,53], which show that shear band emergence precedes the temperature rise. To test whether the configurational softening process is related to cooling history during glass preparation, we carried out additional shear loading simulations on glass samples quenched with different cooling rates. The results are shown in Fig. 8. Figure 8(a) shows that configurational softening process highly depends on the cooling history. For stable glasses quenched with lower cooling rates, the observed rise of configurational temperature is much higher.

The shear banding behavior can be studied in terms of spatial distribution of localized strain, acting as a microscope to visualize the percolation process of shear transformations. Analogous to plastic strain, $\bar{T}_t^i$ and $\bar{T}_c^i$ are continuum fields, being functions of time and position. To clarify, at atomic level, the critical role of configurational softening and thermal softening on the shear band, the projected $\bar{T}_t^i$ and $\bar{T}_c^i$ field at various applied strains are shown in Fig. 3. Here, we track the successive snapshots with strains spanning from 0.1 to 0.114 right before the emergence of shear band. According to Fig. 3, it is intuitive that the configurational temperature distribution within the evolving shear band is initially highly discontinuous, consisting of isolated regions with large configurational temperature. These isolated regions are expected to be responsible for the loss of structural stability, manifesting as activated STZs. Compared with the spatial distribution of configurational temperature, the mapping of atomic thermal temperature is of lower degree of localization and less sensitive to the applied strains before the formation of shear band. Despite the good spatial correspondence between $\bar{T}_t^i$ (or $\bar{T}_c^i$) field and shear banding location at strain of 0.114, the localized degree of distribution of thermal temperature is hastened after the onset of shear band. These results indicate that the configurational softening, with inhomogeneous manner earlier than strain localization, behaves as a driving force of STZ activation and percolation, while the thermal localization is more like the consequence of shear band.

In order to quantitatively exploit the localization behavior of softening process induced by either thermal activation or configurational softening, we calculate the probability distribution of atomic thermal temperature and configurational temperature at various applied strains. The results are shown in Fig. 4. First, we focus on the deformation stages prior to

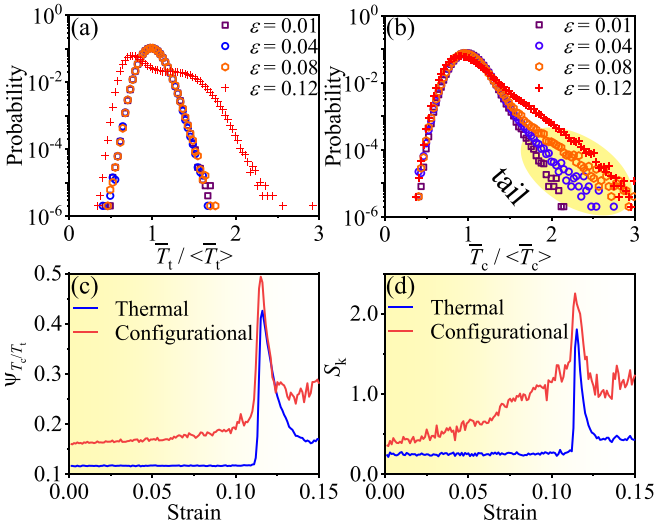

FIG. 4. Inhomogeneous analysis for thermal and configurational softening processes. [(a) and (b)] Statistical distributions of the reduced data normalized by mean value for $\bar{T}_t^i$ as well as $\bar{T}_c^i$ at various applied strains. (c) The evolution of the degree of localization parameter. Here Ψ_{T_t} corresponds to thermal softening while Ψ_{T_c} is related to configurational softening. (d) The skewness of the non-Gaussian profile as a function of applied strains for $\bar{T}_t^i$ and $\bar{T}_c^i$ field.

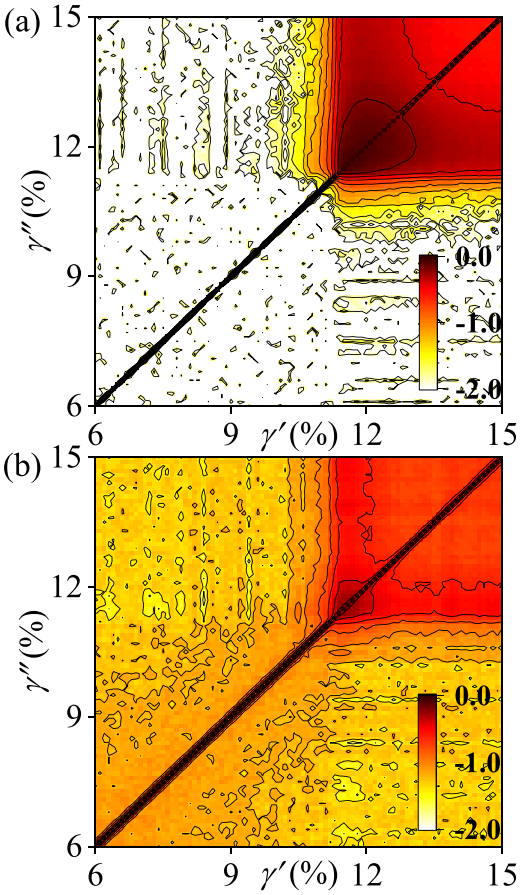

FIG. 5. Correlation matrix $\mathrm{CM}(\gamma', \gamma'')$ of $Cu_{50}Zr_{50}$ MG under shear loading. The color coding corresponds to values of $\mathrm{CM}(\gamma', \gamma'')$ for $\bar{T}_t^i$ (a) and $\bar{T}_c^i$ (b).

shear banding. Intuitively, when $\bar{T}_t^i$ is normalized by its mean value $\langle \bar{T}_t^i \rangle$, the data points overlap with each other and thus collapse onto a single curve. This implies that prior to shear banding emergence the atoms are able to rearrange themselves to maintain a uniform-like distributed temperature field. The distribution of $\bar{T}_t^i$ will not show visible non-Gaussian behavior until shear banding formation. This observation reinforces that heat localization is actually consequence of shear banding. However, we find the striking long-tail distribution of $\bar{T}_c^i$ during the whole deformation process in Fig. 4(b). The extreme $\bar{T}_c^i$ burst is about 3 times the system average. For amorphous solid, local strain fields with a Gaussian core and non-Gaussian tails have been used to account for plastic heterogeneity [48]. In this sense, it is reasonable to speculate that the non-Gaussian distribution of $\bar{T}_c^i$ is closely correlated with extreme values of local strain bursts that are not readily accommodated by immediate surroundings, acting as the origin of shear transformation events and ultimate shear banding. See Fig. 4(b), the tail behavior becomes more pronounced with increasing shear strain indicating more atoms are involved in the inhomogeneous manner.

To more intuitively and straightforwardly evaluate the inhomogeneous manner of $\bar{T}_t^i$ and $\bar{T}_c^i$ field, two quantitative parameters are proposed. The first is the localization parameter which is previously introduced in Ref. [43] to measure stress and strain localization. It has the form of $\psi_{T_c/T_t} = \sqrt{\frac{1}{N}\sum_i \left(\frac{\bar{T}^i}{\langle \bar{T}^i \rangle} - 1\right)^2}$, where $\langle \bar{T}^i \rangle$ is the mean value of $\bar{T}_t^i$ or $\bar{T}_c^i$ and N is the total number of atoms. In this work, we further introduce a new inhomogeneous factor called skewness. It is defined as $S_k = \langle \left(\frac{\bar{T}^i - \langle \bar{T}^i \rangle}{\sigma}\right)^3 \rangle$ with σ denoting the standard deviation. Large values of these two parameters are closely correlated to large fluctuations in the $\bar{T}_t^i$ or $\bar{T}_c^i$ field and hence an increased heterogeneity. Here we plot the results of inhomogeneous analysis in Figs. 4(c) and 4(d). As expected, the heterogeneity of $\bar{T}_c^i$ displays drastic rise in the elastic regime while $\bar{T}_t^i$ exhibits obvious variations only in the stage of strain yielding when a shear band initiates. This physical image is more impressive in Fig. 4(d). It suggests that, when compared with localization parameter ψ, skewness S_k is able to catch asymmetric manner of distributions and hence, is more susceptible to distributions with long tails.

We also calculate the two-time correlation of the $\bar{T}_t^i$ and $\bar{T}_c^i$ field to test the accumulated effect of localized softening events induced by heat and structural disordering, respectively. To address this issue, we define the following "correlation matrix" (CM):

$$\mathrm{CM}(\gamma', \gamma'') = \log\left\{\frac{\langle [P_i(\gamma') - \langle P_i(\gamma') \rangle][P_i(\gamma'') - \langle P_i(\gamma'') \rangle] \rangle}{\sigma(P_i(\gamma'))\sigma(P_i(\gamma''))}\right\}, \quad (6)$$

where $P_i(\gamma')$ represents the physical entity P for atom i at sample strain γ'. Here $\langle\rangle$ denotes statistical average of the system and σ is the standard deviation. It is actually the log-form of Pearson's correlation coefficient. By this definition, larger values of $\mathrm{CM}(\gamma', \gamma'')$ indicate stronger correlation between $P_i(\gamma')$ and $P_i(\gamma'')$. By replacing P with $\bar{T}_t^i$ or $\bar{T}_c^i$, CM then provides a measure of dependence of further softening events

on the existing localized ones. The hidden physical origin is that any irreversible plastic rearrangement (at strain γ') due to thermal activation or configurational softening would be memorized by the following configurations (at strain γ''). The existing localized regions with huge structural rearrangement, would be more soft and thus susceptible to accommodate further distortion, causing accumulation and percolation of shear transformations in these regions. Therefore, high CM values can quantify the accumulated effect of softening and identify the irreversible softening events. As these softening events aggregate into clusters or percolate to form shear bands, the material weakening becomes more pronounced manifesting as increasing values of CM.

Figure 5 presents CM diagrams for thermal and configurational softening process, with darker areas corresponding to higher values of CM. Intuitively, one can see the continuous evolution of CM for $\bar{T}_c^i$ with dark areas showing strong preference of clustering at small sample strains. However, the pattern is quite distinct for $\bar{T}_t^i$, as shown in Fig. 3(a) where dark region is only obvious after yielding. This result shows that irreversible rise of $\bar{T}_c^i$ occurs at early deformation stages acting as the root cause of shear banding, while the subsequent thermal softening events are indeed its consequence.

IV. CONCLUSION

In summary, the configurational temperature and thermal temperature are defined onto single particle to investigate the atomic level softening mechanism of shear banding. Based on these innovative definitions, the hidden softening history, with unprecedented spatial and temporal resolution is revealed. Our results indicate that the softening induced by structural disordering is dominant over the heat effect. Besides, the configurational softening is found to take place much earlier than the rise of thermal temperature. Thus, it is suggested that shear-induced structural disordering, rather than thermally activated diffusion, is the nature of shear banding. Especially under dynamic strain rate, the slow thermal softening process will be suppressed due to the short timescale of deformation. Moreover, our analysis of inhomogeneous fields of configurational temperature and thermal temperature gives the direct evidence that strain localization pop up at softening spots which have undergone irreversible increase of configurational temperature. However, the localization of thermal temperature is found to take place after the onset of shear banding. Thus, it is concluded that the rise of local configurational temperature, as the root cause of locally material weakening, controls shear banding process, while local heating, acting as the consequence, remarkably depends on the evolution of such localization behavior.

What is more surprising is that the rise of configurational temperature in the shear band, at the onset of yielding, reaches nearly 750 K, just beyond the glass transition temperature of $Cu_{50}Zr_{50}$. This observation suggests that the mechanical failure as the form of shear banding is indeed the glass-liquid transition induced by configurational softening. It also supports us to understand the microscopic mechanism of deformation in metallic glasses from the perspective of glass transition. Actually, it is a long-standing goal in the research of metallic glasses community to establish the link between plastic flow like shear banding phenomenon and glass transition theory. In this connection, many pioneering works [23,54,55] have been made to theoretically demonstrate that applied stress activates particle rearrangements causing the mechanical plastic flow, much as thermal fluctuations do in an equilibrium liquid. Besides, it is noteworthy that the excellent simulation work [22] has also pointed out the nontrivial correlation between the plastic flow behavior and glass transition by reporting the similar level of local yield stress in postyield states and the inherent states of liquids equilibrated at the temperature which is slightly higher than the glass transition temperature. Here, our simulation result gives the direct atomic level evidence which supports this point.

As our method of calculating configurational temperature relies on local structure alone, it can also benefit for better understanding the structural origins of deformation and relaxation for metallic glasses and other disordered materials. When used as a structural indicator to represent the glass state, the local configurational temperature takes a step over the fictive temperature by incorporating structural survey information obtained from configurational entropy, which is meaningful to reflect the level of structural disordering in a local region. Such strategy of integration of structural and dynamic features have been validated useful by the success of the flexibility volume [56–58] as an effective signature of glass dynamics.

ACKNOWLEDGMENTS

This work is financially supported by the NSFC Basic Science Center Program for "Multiscale Problems in Nonlinear Mechanics" (Grant No. 11988102), the NSFC (Grant No. 11790292), the National Key Research and Development Program of China (Grant No. 2017YFB0702003). This work is also supported by the Strategic Priority Research Program (Grant No. XDB22040302, XDB22040303), the Key Research Program of Frontier Sciences (Grant No. QYZDJSSW-JSC011).

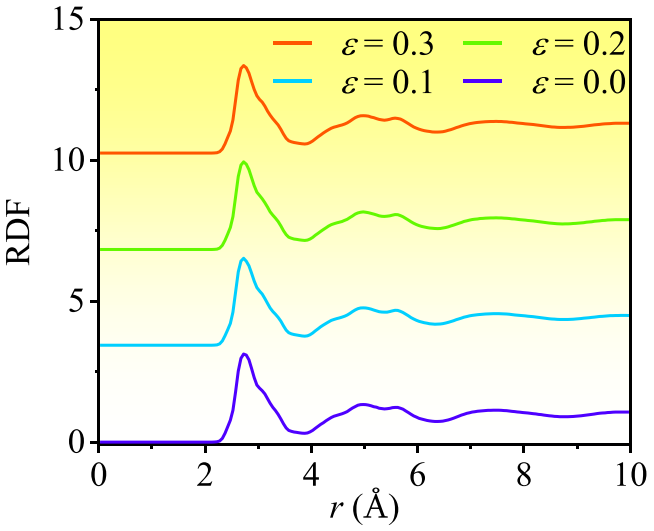

FIG. 6. The radial distribution functions at different levels of macroscopic strain.

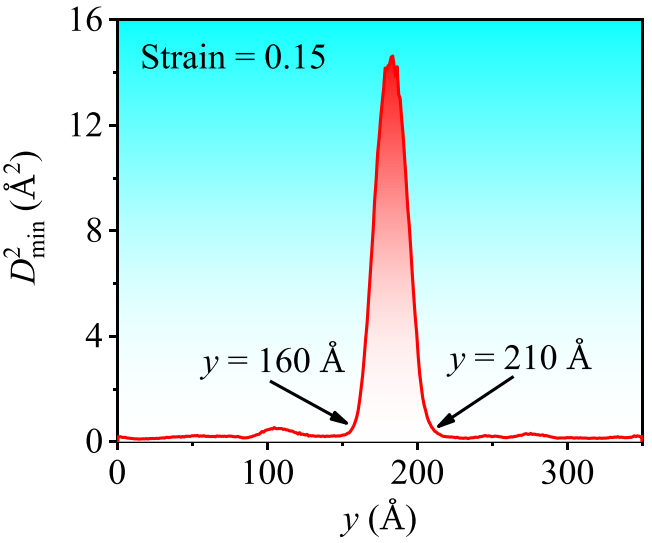

FIG. 7. Spatial distribution of nonaffine displacement along direction of y axis. The data is obtained from snapshot at strain of 0.15 when mature shear band has already formed. Here 160 Å $< y <$ 210 Å denotes the position of shear band.

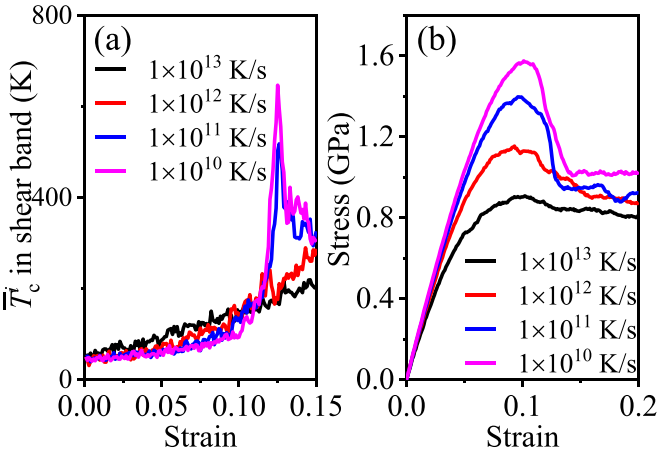

FIG. 8. (a) Evolution of configurational temperature in the shear band against variation in cooling history. (b) Shear stress-strain curves of $Cu_{50}Zr_{50}$ samples with different cooling rates. The cooling rates applied during sample preparation are varying from 1×10^{10} to 1×10^{13} K/s.

APPENDIX A: RADIAL DISTRIBUTION OF THE $Cu_{50}Zr_{50}$ METALLIC GLASS

Figure 6 shows the radial distribution functions of $Cu_{50}Zr_{50}$ metallic glass at various sample strains. It indicates that configurations under different levels of macroscopic strain exhibit similar radial distribution functions with the exact same positions of the first and second peak. As mentioned above, the cutoff distance in Eq. (3) is chosen to be 6 Å, which corresponds to the second valley of RDF. Thus our spatial coarse graining procedure contains the short as well as medium range order of $Cu_{50}Zr_{50}$ glass.

APPENDIX B: IDENTIFICATION OF SHEAR BAND REGION

The minimum nonaffine squared displacement [4] is used to quantify the local plastic deformation. Its definition is

$$D^2_{\min} = \frac{1}{N_i}\sum_j [\vec{d}_{ij}(t+\Delta t) - \mathbf{F}_i\vec{d}_{ij}(t)]^2, \qquad \text{(B1)}$$

where N_i is the number of neighboring atoms around central atom i. $\vec{d}_{ij}$ is the center to center position vector between central atom i and its neighboring jth atom. $\mathbf{F}_i$ denotes the local deformation gradient. t and Δt are time and time interval, respectively. In order to precisely capture the location of shear band, we plot the spatial distribution of $D^2_{\min}$ along direction of y axis, as shown in Fig. 7. It is noticed that mostly deformed atoms with high values of $D^2_{\min}$ locate at regions of 160 Å $< y <$ 210 Å, which is actually the position of shear band.

APPENDIX C: DIFFERENT COOLING RATES

We cast additional shear loading tests on glass samples quenched with different cooling rates, spanning from 1×10^{10} to 1×10^{13} K/s. Figure 8 shows the simulation results. We calculate the rise of configurational temperature for atoms in the shear band. As shown in Fig. 8(a), configurational softening process is highly related to the cooling history, with glasses having lower cooling rates undertaking much higher value of configurational temperature. It should be noted that there are no obvious shear band regions for glass samples with cooling rates of 1×10^{12} and 1×10^{13} K/s, thus the results for these two cases are calculated from atoms in a randomly chosen band region. In Fig. 8(b), it is interesting to notice that glasses quenched with higher cooling rates will have much lower level of stress overshoot. In our previous work [59], we have clarified the inverse proportionality between cooling rates and stress overshoot (or shear band susceptibility). Thus, it can be concluded here that glasses quenched with low cooling rates will exhibit strong localization of configurational softening as well as enhanced shear band susceptibility.

[1] M. L. Falk and J. Langer, Annu. Rev. Condens. Matter Phys. **2**, 353 (2011).
[2] A. Greer, Y. Cheng, and E. Ma, Mater. Sci. Eng. R **74**, 71 (2013).
[3] A. S. Argon, Acta Metall. **27**, 47 (1979).
[4] M. L. Falk and J. S. Langer, Phys. Rev. E **57**, 7192 (1998).
[5] Z. L. Tian, Y. J. Wang, Y. Chen, and L. H. Dai, Phys. Rev. B **96**, 094103 (2017).
[6] D. Sopu, A. Stukowski, M. Stoica, and S. Scudino, Phys. Rev. Lett. **119**, 195503 (2017).
[7] B. Dodd and Y. Bai, *Adiabatic Shear Localization*, 2nd ed. (Elsevier, Oxford, 2012).

[8] H. J. Leamy, T. T. Wang, and H. S. Chen, Metall. Mater. Trans. B **3**, 699 (1972).
[9] F. Spaepen, Acta Metall. **25**, 407 (1977).
[10] J. S. Langer, Phys. Rev. E **70**, 041502 (2004).
[11] M. L. Manning, J. S. Langer, and J. M. Carlson, Phys. Rev. E **76**, 056106 (2007).
[12] E. Bouchbinder and J. S. Langer, Phys. Rev. E **80**, 031132 (2009).
[13] E. Bouchbinder and J. S. Langer, Phys. Rev. Lett. **106**, 148301 (2011).
[14] K. Kamrin and E. Bouchbinder, J. Mech. Phys. Solids **73**, 269 (2014).
[15] L. H. Dai and Y. L. Bai, Int. J. Impact Eng. **35**, 704 (2008).
[16] M. Q. Jiang and L. H. Dai, J. Mech. Phys. Solids **57**, 1267 (2009).
[17] R. Huang, Z. Suo, J. H. Prevost, and W. D. Nix, J. Mech. Phys. Solids **50**, 1011 (2002).
[18] D. D. E. Brennhaugen, K. Georgarakis, Y. Yokoyama, K. S. Nakayama, L. Arnberg, and R. E. Aune, Sci. Rep. **8**, 16317 (2018).
[19] W. J. Wright, R. B. Schwarz, and W. D. Nix, Mater. Sci. Eng. A **319-321**, 229 (2001).
[20] J. J. Lewandowski and A. L. Greer, Nat. Mater. **5**, 15 (2006).
[21] F. Spaepen, Nat. Mater. **5**, 7 (2006).
[22] A. Barbot, M. Lerbinger, A. Lemaître, D. Vandembroucq, and S. Patinet, Phys. Rev. E **101**, 033001 (2020).
[23] T. K. Haxton and A. J. Liu, Phys. Rev. Lett. **99**, 195701 (2007).
[24] G. Kumar, P. Neibecker, Y. H. Liu, and J. Schroers, Nat. Commun. **4**, 1536 (2013).
[25] S. Plimpton, J. Comput. Phys. **117**, 1 (1995).
[26] M. I. Mendelev, M. J. Kramer, R. T. Ott, and D. J. Sordelet, Philos. Mag. **89**, 109 (2009).
[27] S. Nosé, J. Chem. Phys. **81**, 511 (1984).
[28] N. P. Bailey, J. Schiøtz, and K. W. Jacobsen, Phys. Rev. B **73**, 064108 (2006).
[29] Y. Q. Cheng, A. J. Cao, H. W. Sheng, and E. Ma, Acta Mater. **56**, 5263 (2008).
[30] M. H. Yang, B. Cai, Y. Sun, F. Zhang, Y. F. Wang, C. Z. Wang, and K. M. Ho, Phys. Rev. Mater. **3**, 125602 (2019).
[31] M. Singh, M. Ozawa, and L. Berthier, Phys. Rev. Mater. **4**, 025603 (2020).
[32] H. L. Peng, M. Z. Li, and W. H. Wang, Phys. Rev. Lett. **106**, 135503 (2011).
[33] X. Yang, R. Liu, M. Yang, W.-H. Wang, and K. Chen, Phys. Rev. Lett. **116**, 238003 (2016).
[34] J. Ding, S. Patinet, M. L. Falk, Y. Cheng, and E. Ma, Proc. Natl. Acad. Sci. USA **111**, 14052 (2014).
[35] B. Xu, M. L. Falk, J. F. Li, and L. T. Kong, Phys. Rev. Lett. **120**, 125503 (2018).
[36] V. Schmidt, H. Rösner, M. Peterlechner, G. Wilde, and P. M. Voyles, Phys. Rev. Lett. **115**, 035501 (2015).
[37] H. Tong and H. Tanaka, Phys. Rev. X **8**, 011041 (2018).
[38] H. Tong and H. Tanaka, Phys. Rev. Lett. **124**, 225501 (2020).
[39] P. M. Piaggi and M. Parrinello, J. Chem. Phys. **147**, 114112 (2017).
[40] R. E. Nettleton and M. S. Green, J. Chem. Phys. **29**, 1365 (1958).
[41] A. Baranyai and D. J. Evans, Phys. Rev. A **40**, 3817 (1989).
[42] D. Richard, M. Ozawa, S. Patinet, E. Stanifer, B. Shang, S. A. Ridout, B. Xu, G. Zhang, P. K. Morse, J.-L. Barrat, L. Berthier, M. L. Falk, P. Guan, A. J. Liu, K. Martens, S. Sastry, D. Vandembroucq, E. Lerner, and M. L. Manning, Phys. Rev. Mater. **4**, 113609 (2020).
[43] D. Sopu, F. Moitzi, N. Mousseau, and J. Eckert, Appl. Mater. Today **21**, 100828 (2020).
[44] L. Berthier and J.-L. Barrat, Phys. Rev. Lett. **89**, 095702 (2002).
[45] V. Lubchenko and P. G. Wolynes, J. Chem. Phys. **121**, 2852 (2004).
[46] H. A. Makse and J. Kurchan, Nature (London) **415**, 614 (2002).
[47] P. Cao, K. A. Dahmen, A. Kushima, W. J. Wright, H. S. Park, M. P. Short, and S. Yip, J. Mech. Phys. Solids **114**, 158 (2018).
[48] P. Cao, M. P. Short, and S. Yip, Proc. Natl. Acad. Sci. USA **116**, 18790 (2019).
[49] S. Patinet, D. Vandembroucq, and M. L. Falk, Phys. Rev. Lett. **117**, 045501 (2016).
[50] A. Barbot, M. Lerbinger, A. Hernandez-Garcia, R. García-García, M. L. Falk, D. Vandembroucq, and S. Patinet, Phys. Rev. E **97**, 033001 (2018).
[51] S. Patinet, A. Barbot, M. Lerbinger, D. Vandembroucq, and A. Lemaître, Phys. Rev. Lett. **124**, 205503 (2020).
[52] D. Rittel, P. Landau, and A. Venkert, Phys. Rev. Lett. **101**, 165501 (2008).
[53] Y. Guo, Q. Ruan, S. Zhu, Q. Wei, H. Chen, J. Lu, B. Hu, X. Wu, Y. Li, and D. Fang, Phys. Rev. Lett. **122**, 015503 (2019).
[54] Y. H. Liu, C. T. Liu, W. H. Wang, A. Inoue, T. Sakurai, and M. W. Chen, Phys. Rev. Lett. **103**, 065504 (2009).
[55] P. Guan, M. Chen, and T. Egami, Phys. Rev. Lett. **104**, 205701 (2010).
[56] J. Ding, Y.-Q. Cheng, H. Sheng, M. Asta, R. O. Ritchie, and E. Ma, Nat. Commun. **7**, 13733 (2016).
[57] Z. Fan, J. Ding, Q.-J. Li, and E. Ma, Phys. Rev. B **95**, 144211 (2017).
[58] Q. Wang, J. Ding, L. Zhang, E. Podryabinkin, A. Shapeev, and E. Ma, npj Comput. Mater. **6**, 194 (2020).
[59] Z.-Y. Yang, Y.-J. Wang, and L.-H. Dai, Scr. Mater. **162**, 141 (2019).